

## Large area 50 nm period grating by multiple nanoimprint lithography and spatial frequency doubling

Bo Cui, Zhaoning Yu, Haixiong Ge, and Stephen Y. Chou<sup>a)</sup>

*NanoStructure Laboratory, Department of Electrical Engineering, Princeton University, Princeton, New Jersey 08544*

(Received 15 August 2006; accepted 5 October 2006; published online 25 January 2007)

The authors have developed an approach to fabricate large area 50 nm period gratings (22 nm linewidth) with low cost. The method used a fabrication cycle twice, each combining nanoimprint lithography with a spatial frequency doubling based on electroless plating, lift-off, and reactive ion etching. Hence by frequency doubling twice, we started with a 200 nm period grating mold and finished with a 50 nm period grating with a uniform area of 3 cm<sup>2</sup>—the largest achieved today. This method is scalable for the fabrication of even smaller period gratings over a large area, and is a viable low-cost technique for making nanoimprint lithography molds for high-throughput fabrication of 50 nm period grating or grid devices. © 2007 American Institute of Physics.

[DOI: 10.1063/1.2390652]

Large area sub-200-nm period grating or grid structures have many applications, such as in deep-ultraviolet polarizers<sup>1</sup> and transmission or reflection filters,<sup>2,3</sup> broadband antireflection surfaces where the grating linewidth (or grid pillar diameter) increases gradually with depth,<sup>4</sup> high density patterned magnetic data storage media<sup>5</sup> or nonvolatile magnetoresistive random access memory,<sup>6</sup> nanofluidic channels to stretch, align, or sort genomic DNA,<sup>7</sup> array of field emitters for flat-panel display,<sup>8</sup> and atom beam or x-ray diffraction.<sup>9,10</sup> They are also used for fundamental research.

Previous fabrication methods for sub-200-nm grating include electron-beam lithography, electron holographic lithography,<sup>11</sup> and extreme ultraviolet interferometry.<sup>12,13</sup> However, besides being expensive, they all have limited field size and low throughput, and are difficult to extend to large areas. Achromatic interferometric lithography<sup>14</sup> is capable of producing large area 100 nm period gratings with high throughput, yet it is complex in tools and processes, and has not generated gratings of 50 nm period or smaller.

An alternative fabrication technique that can relax the lithography requirement is the “frequency doubling,” which doubles the number of lines of a grating fabricated by other methods.<sup>15–18</sup> A frequency doubling has been reported for fabricating large area 100 nm period grating from a 200 nm period grating.<sup>19</sup> However, the frequency doubling process can be lengthy, hence reducing the yield and increasing the cost. In this letter, we present an approach to double the grating frequency. Compared with previous frequency doubling method, the present one offers far better control of grating periodicity because of two innovations: (a) the use of electroless plating to precisely control the line/gap width [using feedback from scanning electron microscopy (SEM) measurements, one can easily adjust the line/gap width by removing plated materials and replating] and (b) the use of nanoimprint lithography (NIL) [which has shown pattern duplication of 6 nm half pitch<sup>20</sup>] to achieve high fidelity and high-yield pattern duplication for multiple frequency doubling. The frequency doubling process was carried out twice

to achieve a 50 nm period grating from a 200 nm period grating.

The details of the frequency doubling procedure are shown in Fig. 1. For making a 100 nm period grating, we started with a 200 nm period grating in SiO<sub>2</sub> grown on 4 in. Si wafer, generated by interference lithography or nanoimprint lithography. The grating was duplicated in the SiO<sub>2</sub> layer of another Si wafer using NIL, lift-off, and reactive ion etching (RIE). Then the 200 nm period grating lines were narrowed by HF wet etch to a width  $W$ , which is about half

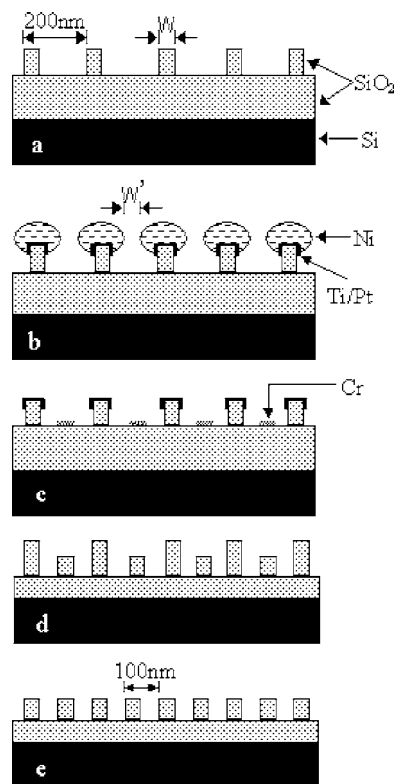


FIG. 1. Schematic of 100 nm period grating fabrication by spatial frequency doubling: (a) 200 nm period grating with narrow line by NIL; (b) Ti/Pt catalyst layer deposition and electroless Ni plating; (c) Cr evaporation and lift-off by Ni in nitric acid; (d) SiO<sub>2</sub> RIE and metal wet-etch removal; (e) planarization by polymer spun-on and etch-back.

<sup>a)</sup> Author to whom correspondence should be addressed; electronic mail: chou@princeton.edu

TABLE I. Electroless Ni plating solution formulation. It has been diluted to 40% that of designed strength to reduce the plating rate for better deposition control.

$\text{NiSO}_4 \cdot 6\text{H}_2\text{O}$	16 g/l
Na citrate	10 g/l
DMAB	0.2 g/l
Thiourea	0.8 mg/l
pH ( $\text{NH}_4\text{OH}$ )	8.5
Temperature	65 °C
Boron in deposit	<0.7%
Plating rate	~30 nm/min

of the final grating period (50 nm in this case). Next, a thin Ti/Pt (adhesion/catalyst, total 3 nm) layer was angle evaporated from both sides of the grating to cover the upper part of the  $\text{SiO}_2$  line. Ni was deposited electrolessly at a rate of 30 nm/min, which formed “mushrooms” on the grating line. The size of the mushroom was controlled so that the gap between the mushrooms,  $W'$ , is equal to  $W$ . With the assistance of SEM measurements, we have achieved near identical  $W$  and  $W'$  (within 5 nm). Thirdly, 10 nm Cr was evaporated at an incident angle normal to the wafer. The openings between adjacent mushrooms allowed the Cr to be deposited onto the bottom of the  $\text{SiO}_2$  trenches. Then Ni mushrooms were dissolved in diluted nitric acid (Ti/Pt not attacked) to lift off the Cr deposited on top of the mushroom. The Cr in  $\text{SiO}_2$  trenches interdigitated with the original  $\text{SiO}_2$  grating to form a new grating with half of the original period (doubled frequency). The Cr grating and  $\text{SiO}_2$  grating (will be etched) served as a RIE mask in a  $\text{CHF}_3/\text{O}_2$  RIE to transfer the pattern into the underneath  $\text{SiO}_2$ . Then Cr, Ti, and Pt were wet etched away using commercial Cr photomask etchant, 1:100 diluted HF (etched negligible oxide), and hot  $\text{HNO}_3:\text{HCl}:\text{H}_2\text{O}=1:7:10$ , respectively. Finally, the wafer surface was planarized by the conventional polymer spun-on and plasma etch-back technique. The polymer was customer developed in house that could achieve the same RIE etching rate as  $\text{SiO}_2$  by adjusting the partial gas pressure of  $\text{O}_2$  and  $\text{CHF}_3$ . The polymer was completely removed by  $\text{O}_2$  plasma afterward.

The electroless plating solution formulation is shown in Table I. Both thickness uniformity and line edge smoothness are critical for the frequency doubling process. The plated Ni was found to be smooth. To achieve uniform deposition, the electroless plating must start simultaneously everywhere, and the deposition rate should be constant across the wafer. We chose dimethyl amine borane (DMAB) as reducing agent because, with the same substrate preparation procedure, we found that the plating was easier to start simultaneously with DMAB than with other reducing agents. As for the deposition rate, electroless plating (as a chemical process) is intrinsically much more uniform than electrical plating, especially when the deposition rate is limited by chemical reaction rate. Figure 2 shows film thickness uniformity over 4 in. silicon wafer coated with Ti/Pt. The plating was performed in an ultrasonic tank for improving film uniformity and a fast removal of generated  $\text{H}_2$  gas to eliminate pinholes. The film thickness was within a 5% variation on area within 4 cm from the wafer center, but became thicker on the wafer edge. This indicates that mass diffusion rate, determined by reactant concentration and solution agitation, still played an important role in determining the plating rate. By attaching the

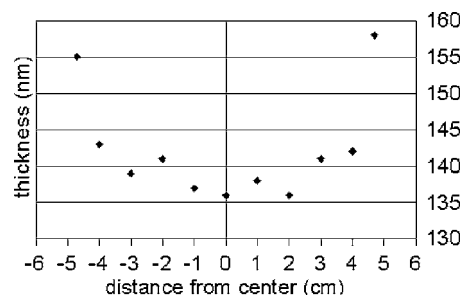


FIG. 2. Electroless Ni film uniformity over 4 in. Si wafer coated with Ti/Pt. Thickness is measured by AFM.

sample to a larger sacrificial wafer, one can reduce the edge effect considerably.

Figure 3 shows the fabricated 100 nm period grating from a 200 nm period NIL mold together with SEM images after two intermediate steps. Electroless Ni plating onto the 200 nm period grating is shown in Fig. 3(a). As expected, the electroless Ni covered only the upper part of the grating lines where Ti/Pt were coated, forming a mushroom profile. Cr was then evaporated onto this grating at normal incident angle. SEM image [Fig. 3(b)] shows that the Cr on trench bottom was disconnected from the Cr on top of Ni; hence the subsequent Cr lift-off in nitric acid was straightforward. Figure 3(c) shows the completed 100 nm period grating with

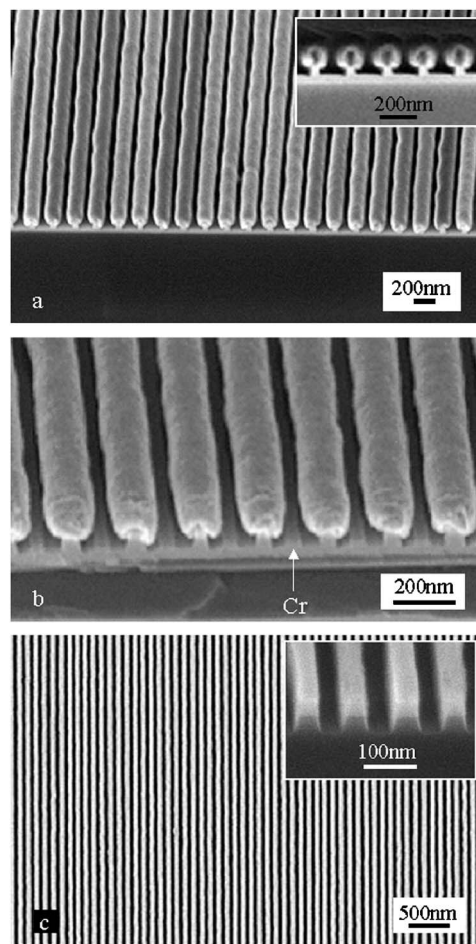


FIG. 3. Fabrication of 100 nm period grating. (a) SEM image after electroless Ni plating. The inset shows the sideview, (b) after Cr evaporation at normal incident angle, and (c) the completed 100 nm period grating with 55 nm linewidth. The inset shows the cross section.

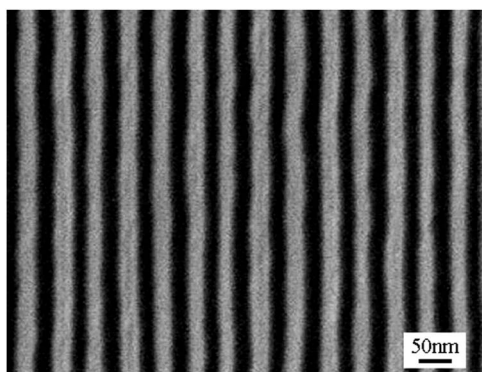


FIG. 4. 50 nm period grating with 22 nm linewidth over a large area fabricated by doubling twice from a 200 nm period grating.

linewidth of 55 nm. The new set of grating lines could not be distinguished from the old set. The surface topology after planarization was measured by atomic force microscopy (AFM) and showed a fluctuation of  $<5$  nm, which is small enough for the grating to be used as a NIL mold. The edges of each line appear a little rough due to the line edge roughness of the original 200 nm period master mold. The uniform area, defined here by 5 nm linewidth difference between the two sets of lines, and limited by the linewidth nonuniformity of the master mold, is  $\sim 10$  cm<sup>2</sup>.

After having the 100 nm period grating, we used it to carry out another cycle of nanoimprint and frequency doubling process to achieve a 50 nm period grating. The completed 50 nm period grating with about 22 nm linewidth is shown in Fig. 4. The line roughness and irregularity of the master 200 nm period grating are further amplified in the 50 nm period case. The uniform area, due to process error and master grating nonuniformity, is reduced to about 3 cm<sup>2</sup>. With better process control, the 50 nm period grating could have a uniform area over 10 cm<sup>2</sup>.

The current fabrication process involves only NIL, electroless plating, metal evaporation and lift-off, and RIE, which are all low-cost processes. In addition, unlike interference lithography, this process is scalable for even smaller

period gratings. Combined with NIL, one would find a number of applications, particularly in the field of patterned magnetic recording media or subwavelength optical devices.

This work was supported in part by ONR and DARPA.

- <sup>1</sup>E. E. Scime, E. A. Anderson, D. J. McComas, and M. L. Schattenburg, *Appl. Opt.* **34**, 648 (1995).
- <sup>2</sup>M. Gruntman, *Appl. Opt.* **34**, 5732 (1995).
- <sup>3</sup>T. M. van Beek, R. C. Fleming, P. S. Hindle, J. D. Prentiss, M. L. Schattenburg, and R. Ritzau, *J. Vac. Sci. Technol. B* **16**, 3911 (1998).
- <sup>4</sup>Y. Ono, Y. Kimura, Y. Ohta, and N. Nishidan, *Appl. Opt.* **26**, 1142 (1987).
- <sup>5</sup>S. Y. Chou, M. S. Wei, P. R. Krauss, and P. B. Fischer, *J. Appl. Phys.* **76**, 6673 (1994); B. Cui, W. Wu, L. Kong, X. Sun, and S. Y. Chou, *ibid.* **85**, 5534 (1999).
- <sup>6</sup>B. Vogeli, H. I. Smith, F. J. Castano, S. Haratani, Y. W. Hao, and C. A. Ross, *J. Vac. Sci. Technol. B* **19**, 2753 (2001).
- <sup>7</sup>R. H. Austin, J. O. Tegenfeldt, H. Cao, S. Y. Chou, and E. C. Cox, *IEEE Trans. Nanotechnol.* **1**, 12 (2002).
- <sup>8</sup>C. O. Bozler, C. T. Harris, S. Rabe, D. D. Rathman, M. A. Hollis, and H. I. Smith, *J. Vac. Sci. Technol. B* **12**, 629 (1994).
- <sup>9</sup>R. E. Grisenti, W. Schöllkopf, J. P. Toennies, J. R. Manson, T. A. Savas, and H. I. Smith, *Phys. Rev. A* **61**, 033608 (2000).
- <sup>10</sup>D. Hambach, G. Schneider, and E. M. Gullikson, *Opt. Lett.* **26**, 1200 (2001).
- <sup>11</sup>K. Ogai, Y. Kirmura, R. Shimizu, J. Fujita, and S. Matsui, *Appl. Phys. Lett.* **66**, 1560 (1995).
- <sup>12</sup>M. G. Capeluto, G. Vaschenko, M. Grisham, M. C. Marconi, S. Ludueña, L. Pietrasanta, Y. Lu, B. Parkinson, and C. S. Menoni, *IEEE Trans. Nanotechnol.* **5**, 3 (2006).
- <sup>13</sup>H. H. Solak, D. He, W. Li, S. S. Gasson, S. S. Cerrina, B. H. Sohn, X. M. Yang, and P. Nealey, *Appl. Phys. Lett.* **75**, 2328 (1999).
- <sup>14</sup>T. A. Savas, M. L. Schattenburg, J. M. Carter, and H. I. Smith, *J. Vac. Sci. Technol. B* **14**, 4167 (1996).
- <sup>15</sup>D. C. Flanders and N. N. Efremow, *J. Vac. Sci. Technol. B* **1**, 1105 (1983).
- <sup>16</sup>L. F. Johnson and K. A. Ingersoll, *Appl. Phys. Lett.* **38**, 532 (1981).
- <sup>17</sup>G. J. Sonek, D. K. Wagner, and J. M. Ballantyne, *J. Vac. Sci. Technol.* **19**, 921 (1981).
- <sup>18</sup>D. C. Flanders and A. E. White, *J. Vac. Sci. Technol.* **19**, 892 (1981).
- <sup>19</sup>Z. Yu, W. Wu, L. Chen, and S. Y. Chou, *J. Vac. Sci. Technol. B* **19**, 2816 (2001).
- <sup>20</sup>M. D. Austin, H. Ge, W. Wu, M. Li, Z. Yu, D. Wasserman, S. A. Lyon, and S. Y. Chou, *Appl. Phys. Lett.* **84**, 5299 (2004); M. D. Austin, W. Zhang, H. Ge, D. Wasserman, S. A. Lyon, and S. Y. Chou, *Nanotechnology* **16**, 1058 (2005).